Spectrochimica Acta Part A: Molecular and Biomolecular Spectroscopy 359 (2026) 127928

Contents lists available at ScienceDirect

Spectrochimica Acta Part A:
Molecular and Biomolecular Spectroscopy

journal homepage: www.journals.elsevier.com/spectrochimica-acta-part-a-molecular-and-biomolecular-spectroscopy

Discrimination of nanovesicles using two-color laser-induced fluorescence detection

Shunsuke Asahi, Takashi Kaneta *

Department of Chemistry, Okayama University, 3-1-1 Tsushimanaka, Kita-ku, Okayama 700-8530, Japan

HIGHLIGHTS

- The method enables the simultaneous detection and discrimination of CD63-positive and non-CD63-positive EVs using dual-laser excitation.
- We validated the detection system using two distinct types of fluorescently labeled liposomes.
- Our results demonstrate that a measurable proportion of CD63-positive EVs remains in the culture medium without preconcentration.
- The method revealed that treatment with doxorubicin increases the release of CD63-positive EVs, even as the total cell number decreases.

GRAPHICAL ABSTRACT

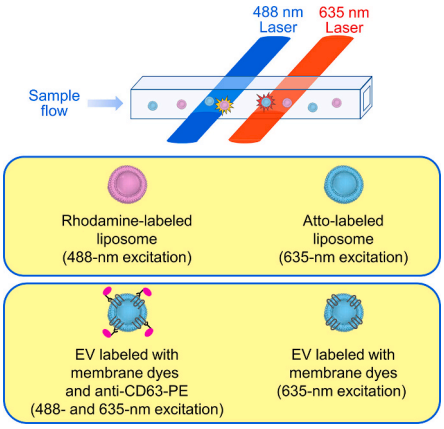

ABSTRACT

A two-color fluorescence-detection system was developed to distinguish between two types of nanovesicles labeled with different fluorescent dyes. This system employs two lasers emitting at distinct wavelengths (488 and 635 nm). These lasers are reshaped into sheet-like beams and focused at separate positions within a square capillary. As vesicles flow through the capillary, they pass through the laser beams and emit fluorescence when excited by the corresponding wavelength. This technique allows for the counting of vesicles and identification of the specific fluorophores on the vesicles based on their emission positions. The system was validated using liposomes labeled with fluorophores excited by the 488 and 635 nm lasers. It was then applied to differentiate CD63-positive extracellular vesicles (EVs) from other types of EVs in a culture media consisting of HeLa and A549 cells. Additionally, the system was used to study the effect of the anticancer drug doxorubicin on EV secretion in these cancer cells.

1. Introduction

Extracellular vesicles (EVs) are particles without a nucleus that are surrounded by lipid bilayer membranes, and they are released by biological cells. EVs are a highly heterogeneous population of lipid bilayer-delimited particles ranging in size from approximately 30 nm to several micrometers. While EVs have often been categorized into subtypes such as exosomes and microvesicles based on their biogenesis, the International Society for Extracellular Vesicles (ISEV) now recommends the use of "small EVs" (sEVs) to describe vesicles typically smaller than 150 or

* Corresponding author.
E-mail address: kaneta@okayama-u.ac.jp (T. Kaneta).

https://doi.org/10.1016/j.saa.2026.127928
Received 9 February 2026; Received in revised form 6 April 2026; Accepted 14 April 2026
Available online 16 April 2026

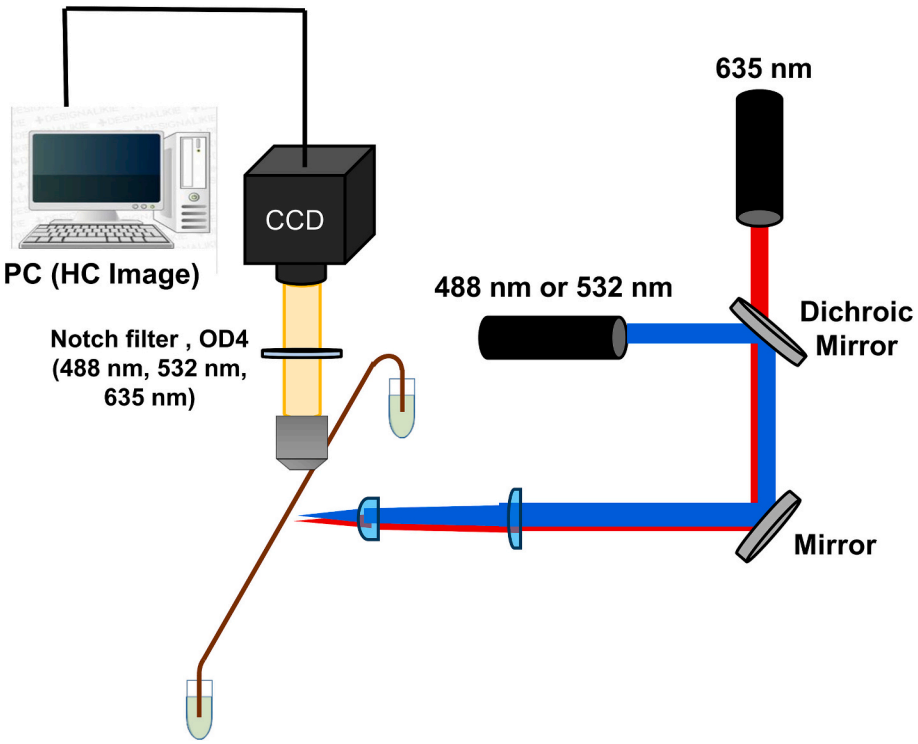

Fig. 1. Schematic illustration of the detection system equipped with two lasers.

200 nm, as specified in the MISEV2023 guidelines [1,2]. Exosomes contain nucleic acids such as mRNA and microRNA and play roles in intercellular communication. Recent studies have suggested that exosomes influence pathological conditions such as the progression of various diseases, cancer tumor growth and metastasis, and resistance to therapy [3–5]. Therefore, exosomes are projected to be useful as diagnostic biomarkers and targeted drug-delivery media that have the potential to lead to clinical applications and preclinical advances. In addition, most bodily fluids such as blood and urine [6] contain exosomes, and issues such as detection and isolation are challenging.

With respect to exosome analysis, however, several challenging issues must be resolved. Many studies have focused on the separation and purification of exosomes in biological fluids that always contain different types of EVs and particles such as microvesicles, apoptotic bodies, and cell debris. Furthermore, plasma lipoproteins, such as low-density lipoproteins, represent major co-isolated contaminants in EV samples derived from biological fluids due to their overlapping physical properties with EVs [7]. The most commonly used methods for collecting exosomes are ultrafiltration and ultracentrifugation [8,9], both of which require expensive instruments, large amounts of samples, and a significant amount of time. Collection is also based either on vesicle density or size, which suggests they contain microvesicles due to their size overlap with exosomes. New developments in microfluidics [10,11], immunomagnetic particles [12], and size exclusion chromatography [13] have, on the other hand, enhanced the numbers and purity of exosomes that can be gathered. We have demonstrated the collection of model vesicles and EVs by radiation pressure, which was enhanced by the presence of gold nanoparticles [14–16]. The collection efficiency of these techniques has remained unclear, however, because of difficulties in directly estimating the exosome concentrations in the original samples. Therefore, it is a challenge to discriminate exosomes from the other vesicles in a mixture [17].

On the other hand, many research groups are actively developing high-performance methods to analyze exosomes. To date, various techniques have been employed for exosome analyses such as nanoparticle tracking analysis (NTA), Western blotting, and flow cytometry. These methods, however, have certain limitations [18]. For example, NTA can generally determine only the size distribution and the population of vesicles without discrimination of the protein biomarkers, Western blotting involves complex procedures such as sample preparation, electrophoresis, blotting, and detection, and flow cytometry requires purified samples. To overcome these limitations, recent studies have introduced more sophisticated and improved analytical methods for EVs, as summarized in several review articles [19–24]. Fluorescence NTA would be a promising technique to detect fluorescently labeled EVs [25]. More recently, two-color fluorescence NTA demonstrated simultaneous determination of two fluorescent labels on nanoparticles [26], although the discrimination of different particles is still challenging. Flow cytometry is also employed for counting EVs. However, flow cytometry generally presents difficulties in the direct measurement of a culture medium by requiring the purification of EVs [27] and using instrumentation that is extremely expensive and therefore difficult to use on a routine basis. Therefore, development of an easy and inexpensive method to discriminate EVs continues to be a challenge.

In this study, we developed a system for quantitatively discriminating two types of nanovesicles. Our proposed system utilizes laser-induced fluorometry via two different excitation wavelengths. The principle was initially validated using two types of liposomes labeled with two types of dye-lipid conjugates that emit at different wavelengths. Since these liposomes have different excitation wavelengths, they are selectively detected using two different lasers. In addition, the proposed system permits the direct counting of EVs in a cell culture medium without the need for time-consuming isolation steps as demonstrated in our previous work [28]. We simultaneously use two distinct approaches to label vesicles in a culture media—one involves binding with a fluorescently labeled antibody that targets a membrane protein specific to some EVs while the other employs a membrane-binding dye that stains all EVs. We attempted to discriminate CD63-positive EVs from all EVs in a culture media.

2. Experimental

2.1. Materials

Ultrapure water was acquired from Milli-Q-Lab (Millipore, Tokyo, Japan). Chloroform, 1 M hydrochloric acid, and 1 M sodium hydroxide solution were purchased from Fujifilm Wako Pure Chemicals (Osaka, Japan). Then, 4-(2-hydroxyethyl)-1-piperazineethanesulfonic acid (HEPES) was obtained from Sigma-Aldrich Japan (Tokyo, Japan). Fluorescently labeled lipid solutions, 0.1 mM 1,2-dipalmitoyl-sn-glycero-3-phosphoethanolamine-N-(lissamine rhodamine B sulfonyl) (Rhod-DPPE) chloroform solution (λex = 555 nm, λem = 580 nm) and 0.5 mM 1,2-dipalmitoyl-sn-glycero-3-phosphoethanolamine labeled with Atto 633 (Atto-DPPE, λex = 630 nm; λem = 651 nm) were purchased from Avanti (AL, USA) and ATTO TEC. (Siegen, Germany), respectively. Unlabeled dipalmitoylphosphatidylcholine (DPPC) for the preparation of liposomes was also obtained from Avanti. HeLa cells (human cervical cancer cells) and A549 cells (human alveolar basal cell carcinoma cells) were obtained from the JCRB cell bank (Tokyo, Japan). Dulbecco's Modified Eagle Medium (DMEM, high glucose), fetal bovine serum, antibiotic-antimyotic, 0.05% trypsin-EDTA, and Dulbecco's phosphate-buffered saline (DPBS) were obtained from Gibco (Thermo Fisher SCIENTIFIC, Tokyo, Japan). A fluorescently labeled anti-CD63 antibody (anti-CD63-phycoerythrin conjugate, anti-CD63-PE, λex = 494 nm and 565 nm; λem = 576 nm) was purchased from Beckman-Coulter (CA, USA). The ExoSparkler exosome membrane labeling kit Deep Red (membrane-labeling dye, λex = 648 nm; λem = 664 nm) was purchased from the Dojin Chemical Laboratory (Kumamoto, Japan). We have confirmed that the fetal bovine serum used in this study did not contain detectable amounts of EVs that could react with anti-CD63-PE before the experiment.

2.2. Apparatus

The configuration of the detection system closely follows a design originally developed by Anazawa et al. [29] for single-molecule detection, which was later adapted by our group for the counting of EVs [28]. The primary difference in the setup of the system proposed in the present study is the use of two lasers to enable discrimination between two types of vesicles. A schematic diagram of the detection system is shown in Fig. 1. Two lasers, operating at wavelengths of 488 nm (20 mW, BioRay laser, Edmund, Tokyo, Japan) and 635 nm (6 mW, semiconductor laser, Sigma Koki, Tokyo, Japan) served as excitation light sources. Each laser beam was reshaped into a sheet-like form using cylindrical lenses and then focused at distinct positions within a square capillary (outer diameter: 363 μm; inner diameter: 75 μm; length: 60 cm; Molex, Kanagawa, Japan). The 488 nm laser beam was shaped to a width of 70 μm and a thickness of 30 μm, while the 635 nm beam measured 140 μm in width and 30 μm in thickness. The 488 and 635 nm laser beams were aligned within the same observation window but positioned in spatially distinct regions. The extent of any overlap was not quantitatively characterized; however, the beams were adjusted to minimize direct overlap. A narrow boundary region could exist between the two excitation areas, where limited contribution from both wavelengths cannot be completely excluded. This condition permitted tracing the trajectory of the vesicles, which were detected in both focusing areas.

To create a detection window, the polyimide coating at the center of the capillary was removed using a flame. With the proposed system, the laser beams pass through separate regions within this window. Scattered laser light is suppressed using a notch filter (StopLine, 488/532/635 OD4 for each wavelength, OPTO-LINE, Inc., Saitama, Japan). Fluorescence emitted within the detection window is observed using an optical microscope equipped with a 20× objective lens and an ORCA-Flash 2.8 CCD camera (Hamamatsu Photonics, Shizuoka, Japan). We used HC Image software provided by Hamamatsu Photonics to analyze the images.

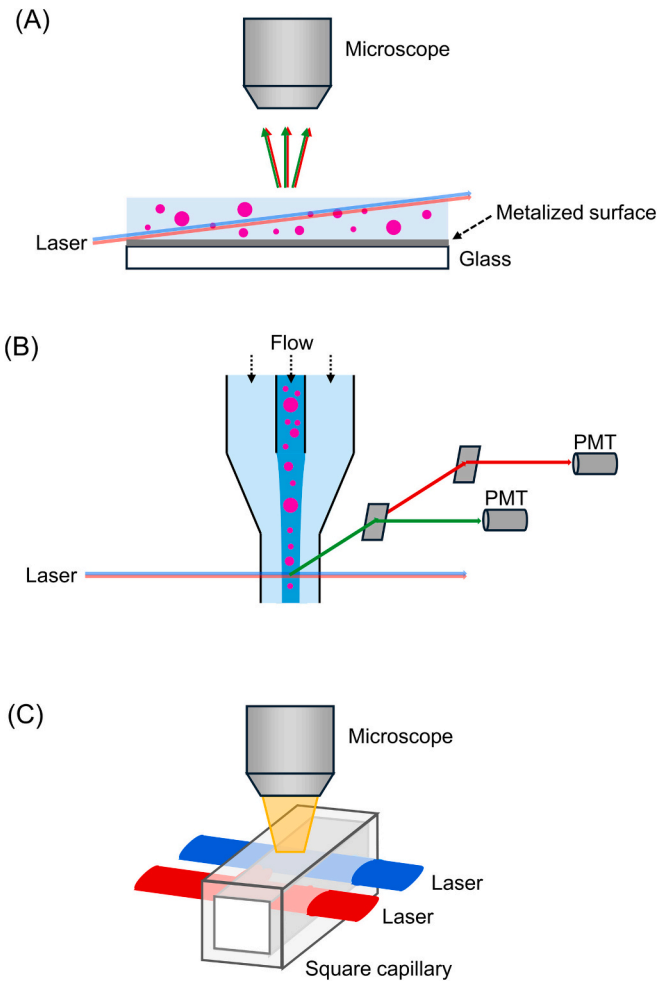

Fig. 2. Schematic illustration of the detection methods for fluorescence nanoparticle tracking analysis, two-color flow cytometry, and the system used in the present study. (A) fluorescence nanoparticle tracking analysis, (B) two-color flow cytometry, (C) the system used in the present study.

To clarify the characteristics of our system, we compared its principle with fluorescence nanoparticle tracking analysis (NTA) and flow cytometry (Fig. 2). While NTA tracks particles based on Brownian motion in a bulk solution, our method utilizes a glass capillary to constrain sample flow, and this ensures that vesicles pass through defined detection regions.

In contrast to conventional flow cytometry, where fluorescence signals are typically detected at a single interrogation point, our system employs two laser beams focused at spatially separated positions. This configuration enables sequential detection of fluorescence signals from individual vesicles, which allows temporal correlation between two colors.

In addition, when compared with commonly used methods, our system allows analysis of EVs with minimal sample processing. In this study, EVs were successfully detected from samples subjected only to low-speed centrifugation. These differences highlight the complementary nature of the present method relative to existing techniques.

2.3. Preparation of fluorescent liposomes and EVs

Fluorescent liposomes were prepared as follows: 7.5 μL of 50 mg mL^{-1} DPPC and 50 μL of 0.125 mg mL^{-1} Rhod-DPPE or Atto-DPPE in chloroform were added to a glass tube. Nitrogen gas was blown into the tube to evaporate the chloroform. The glass tube was then placed in a vacuum desiccator for 1 h to completely remove the chloroform. The

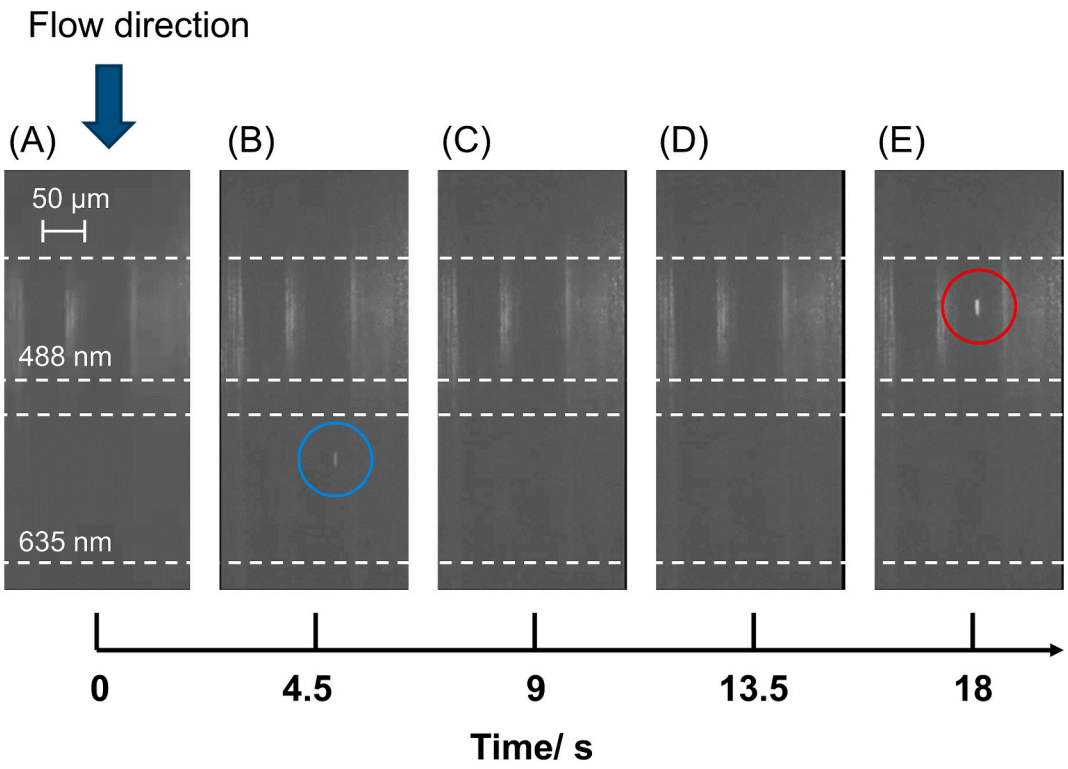

Fig. 3. Time-lapse images of Rhod-labeled and Atto-labeled liposomes. Images are shown at 4.5 s intervals from 0 to 18 s. (A) 0 s, (B), 4.5 s, (C) 9 s, (D), 13.5 s, (E) 18 s.

phospholipid film at the bottom of the glass tube was hydrated with 500 μL of 20 mM HEPES buffer (pH 7.5) at 55 °C in an ultrasonic bath for 30 s. The sizes of the liposomes were adjusted by using an extruder equipped with membrane filters that could be changed to accommodate pore sizes of 100 nm. The details of physicochemical characterizations such as particle size distribution, zeta potential, and fluorescent labeling efficiency were not performed in this study. Fluorescent and non-fluorescent lipids were mixed in a homogeneous chloroform solution prior to liposome formation; therefore, the ratio of fluorescent to non-fluorescent lipids is assumed to be consistent among liposomes.

Two fluorescent liposomes, Rhod-labeled liposomes and Atto-labeled liposomes, were employed to adjust the laser alignment and validate the detection system. The fluorescent liposomes were stained with two dyes and prepared using the same protocol by adding 7.5 μL of 50 mg mL^{-1} DPPC and 25 μL of 0.125 mg mL^{-1} Rhod-DPPE and 25 μL of 0.125 mg mL^{-1} Atto-DPPE.

Two cell lines, HeLa and A549, were used to prepare the medium samples. Initially, the cells were cultured in Petri dishes with 10-cm diameters and subcultured until approximately 100% confluence was reached. Once confluence was achieved, the culture medium was collected in a 15 mL centrifuge tube and centrifuged at 3000 ×*g* for 15 min to concentrate the cell fragments and dead cells as sediment. A 50 μL aliquot of the supernatant was then transferred to a 1.2 mL microtube and mixed with 1.0 μL of anti-CD63-PE. The microtube was shaken at 100 rpm for 1 h at room temperature, which was followed by incubation at 4 °C for an additional hour. Subsequently, 1.5 μL of a membrane-labeling dye was added, and the mixture was incubated at 37 °C for 30 min. Amounts of anti-CD63-PE and the membrane-labeling dye were optimized to obtain the highest fluorescence intensity against the background signal (Ref. 28 for anti-CD63-PE and Supplementary materials, Fig. S1 for the membrane-labeling dye) because all samples contain free anti-CD63-PE and the membrane-labeling dye. Because the EVs used in this study were not fully characterized according to MISEV guidelines such as those prescribed for the Western blotting of EV biomarkers, we refrained from using the term "exosome." Instead, the vesicles are referred to as CD63-positive EVs based on the labeling strategy. The results of transmission electron microscope and nanoparticle tracking analysis for the EVs collected from HeLa cells appear in our previous publication [16].

2.4. Measurement of liposomes and EVs

The excitation and emission characteristics of the fluorescent dyes used in this study are summarized as follows. Rhod-DPPE was excited at 488 nm and emits in the green–orange region, while Atto-DPPE was excited at 635 nm and emits in the red region. Anti-CD63-phycoerythrin (PE) was excited at 488 nm with emission in the orange region. The membrane-labeling dye (ExoSparkler Deep Red) was excited at 635 nm and emits in the far-red region. The corresponding excitation sources (488 and 635 nm lasers) were selected based on these spectral properties. The excitation and emission spectra of anti-CD63-PE and the membrane-labeling dye are shown in Fig. S2 of the Supplementary materials.

Before measurement, the square capillary was manually washed by sequentially flushing it with 0.1 M of HCl, 0.1 M of NaOH, and deionized water using a syringe. The sample—comprised of either fluorescent liposomes or EVs—was introduced by immersing the inlet end of the capillary into a vial containing the sample, while the outlet end was placed in a separate vial filled with water. To induce flow via siphoning, the sample vial was elevated 3 cm above the outlet vial. As the vesicles flowed through the capillary, fluorescence images were captured using a CCD camera with a 200 ms exposure time over a 5-min period. The number of vesicles was then determined by manually counting the fluorescent vesicles in the recorded images.

2.5. Treatment with doxorubicin

HeLa and A549 cells were treated with doxorubicin to assess its effect on the release of EVs. After the cells reached 100% confluence, they were detached from the bottom of the Petri dish by adding 1 mL of

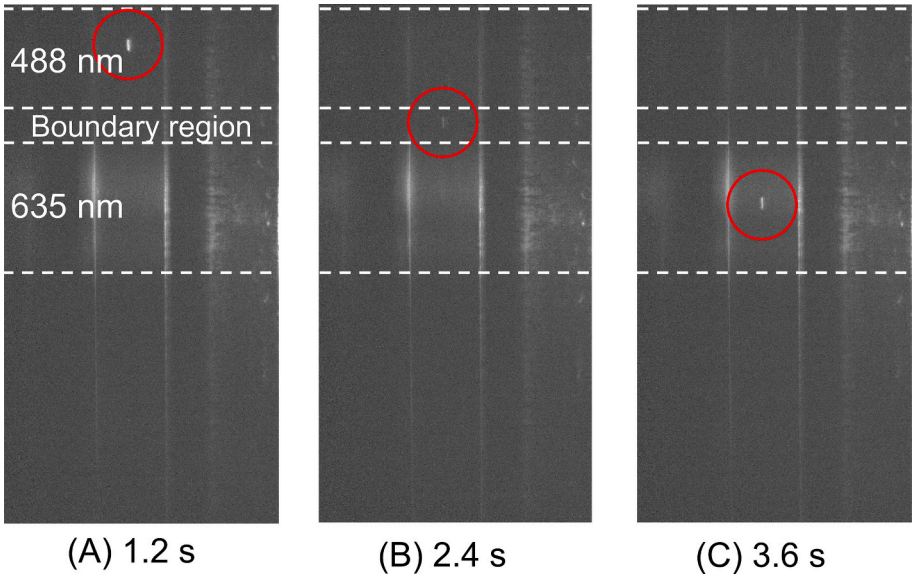

Fig. 4. Images of the trajectory for a liposome labeled with two dyes. The liposome surrounded by a red line emitted at 488 nm of excitation at 1.2 s. The liposome emitted at the boundary region of 488 and 635 nm at 2.4 s. The liposome emitted at 635 nm of excitation at 3.6 s. (For interpretation of the references to color in this figure legend, the reader is referred to the web version of this article.)

EDTA-trypsin, incubating for 5 min, and then adding 9 mL of the culture medium to suspend the cells. A 10 mL aliquot of the cell suspension was seeded in a 10 cm diameter Petri dish containing 9 mL of culture medium. After incubation for 48 h, the cells were washed with DPBS, and a culture medium containing 0.5, 1.5, or 3.0 μM of doxorubicin was added. The cells were incubated in the presence of doxorubicin for 48 h. The EVs were collected from the culture medium and were labeled with anti-CD63-PE and the membrane-labeling dye, as described in the section for the preparation of fluorescent liposomes and EVs.

The number of viable cells was determined using a handheld cell counter (Scepter, Merck Millipore, Japan). After the culture medium was removed, the cells were washed with DPBS and detached from the dish surface using trypsin/EDTA. The collected cells were then resuspended in DPBS, and their number was measured with the handheld cell counter.

3. Results and discussion

3.1. Method validation using fluorescent liposomes

To evaluate the performance of the two-laser detection system, we first attempted to discriminate between two types of liposomes labeled with different fluorescent molecules. Liposomes were selected for this initial validation because they consist of lipid bilayers similar to those of EVs, which includes exosomes. The number of detected liposomes was quantified based on fluorescence signals. Because the analysis focused on relative comparisons, variations in physicochemical properties such as size distribution or zeta potential are unlikely to substantially affect the overall trends. The system successfully detected the two types of liposomes at distinct positions: Rhod-labeled liposomes were detected at the position where the 488 nm laser was focused, while Atto-labeled liposomes were detected at the position where the 635 nm laser was focused.

Fig. 3 shows time-lapse images of the Rhod-labeled and Atto-labeled liposomes detected at different positions within the capillary. The 488 nm laser was focused upstream, while the 635 nm laser was focused downstream, which resulted in the detection of Rhod-labeled liposomes in the upper region of the images and Atto-labeled liposomes in the lower region. Images are shown at 4.5 s intervals from 0 to 18 s (A–E). No liposome was detected at 0 s, whereas an Atto-labeled liposome was detected at 4.5 s (B) in the region irradiated by the 635 nm laser. Subsequently, a Rhod-labeled liposome was detected at 18 s (E) in the region irradiated by the 488 nm laser. The full sequence of this process is provided in Supplementary video S1.

When the liposomes were labeled with fluorescent dyes, fluorescence emissions were observed in regions irradiated by the 488 and 635 nm laser beams. In contrast, no detectable events were observed for the measurements of water (no liposomes) or liposomes without fluorescent labeling, as shown in Fig. S3 of the Supplementary materials.

The detection of a dual-labeled liposome is shown in Fig. 4. The liposome first appeared in the 488 nm excitation region at 1.2 s, subsequently traversed the boundary region of the two laser beams at 2.4 s, and finally entered the 635 nm excitation region at 3.6 s. Due to the partial overlap of the laser beams at their boundaries, the trajectory of the liposome could be continuously tracked as it moved between the excitation zones. This overlap allowed the unambiguous identification of vesicles exhibiting fluorescence under both 488 and 635 nm excitations.

To assess the quantitative performance of the system, liposome solutions were serially diluted and introduced into the capillary. The number of detected liposomes was proportional to the dilution factor for both Rhod-labeled and Atto-labeled liposomes, which demonstrated the system's capability to quantify vesicles labeled with fluorescent dyes in solution (Fig. S4, Supplementary materials). Furthermore, to evaluate the ability of the system to simultaneously quantify two different vesicle types, mixtures containing different ratios of Rhod-labeled and Atto-labeled liposomes were analyzed. As shown in Table 1, mixtures prepared at ratios of 1:1, 1:2, and 2:1 yielded detected liposome counts of 37:45, 33:92, and 65:49, respectively. The observed counts closely matched the expected mixing ratios. The number of Rhod-labeled liposomes did not exactly equal that of Atto-labeled liposomes in the 1:1 sample (37,45). The other mixtures also contained numbers of Atto-labeled liposomes that were slightly larger than the number of Rhod-labeled liposomes that was expected from the mixing ratios. The slight discrepancy in the counted numbers against the mixing ratios was attributed to differences in the initial concentrations of liposomes in the stock solutions. Nevertheless, these results confirm that the detection system allows a researcher to simultaneously quantify and distinguish between two types of vesicles with a high degree of accuracy. In Table 1, the standard deviations for three replicates are less than 7 counts

Table 1
Average number of particles measured in each mixed sample.

Ratio	Number of liposomes (Rhod-labeled)	Number of liposomes (Atto-labeled)
1:1	37 ± 3	45 ± 5
1:2	33 ± 2	92 ± 2
2:1	65 ± 2	49 ± 7

Measurement time, 10 min ($n = 3$).

independent of the total counts. This fact suggests that increasing the counting number of vesicles will improve the relative standard deviations.

A direct comparison with established techniques such as fluorescence NTA and flow cytometry would provide further insight into the performance of the present system. While such experimental validation was not included in this study, differences in excitation geometry and detection principles (shown in Fig. 2) indicate that each method has distinct characteristics. In particular, the present system employs spatially separated excitation, which enables temporal separation of fluorescence signals from different fluorophores.

A limitation of this study is that neither the absolute number and ratio of liposomes nor that of EVs were independently validated using techniques such as NTA, flow cytometry, or electron microscopy. Although liposomes were prepared under controlled conditions with defined compositions, the exact particle number and labeling ratio were not directly measured. Therefore, the present analysis focuses on relative comparisons rather than absolute quantification. Future studies will incorporate complementary techniques to validate particle number and composition.

3.2. *Discrimination of CD63-positive EVs from others*

Biological cells release various types of EVs into a culture medium during their growth process. In the present study, EVs were collected from HeLa cells and A549 cells. Fig. 5 presents a schematic illustration of the labeling system used to discriminate CD63-positive EVs from other EVs. Exosomes generally express CD63, which is a member of the transmembrane-4-superfamily of tetraspanin proteins that are abundantly present on the surface of exosomes. Due to generally high levels of expression, CD63 is one of the representative proteins frequently

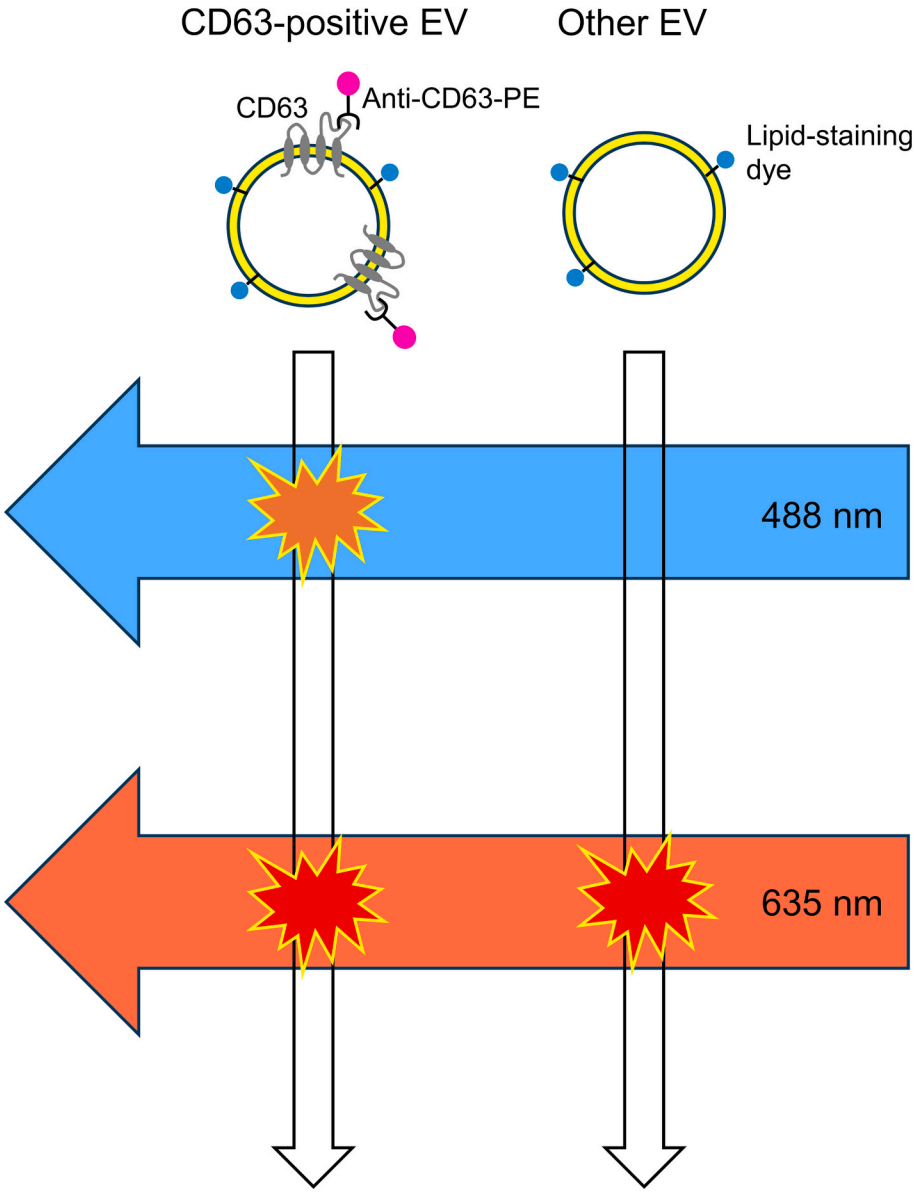

Fig. 5. Schematic illustration of the principle used to discriminate CD63-positive EVs from "other" types of EVs via different labeling methods.

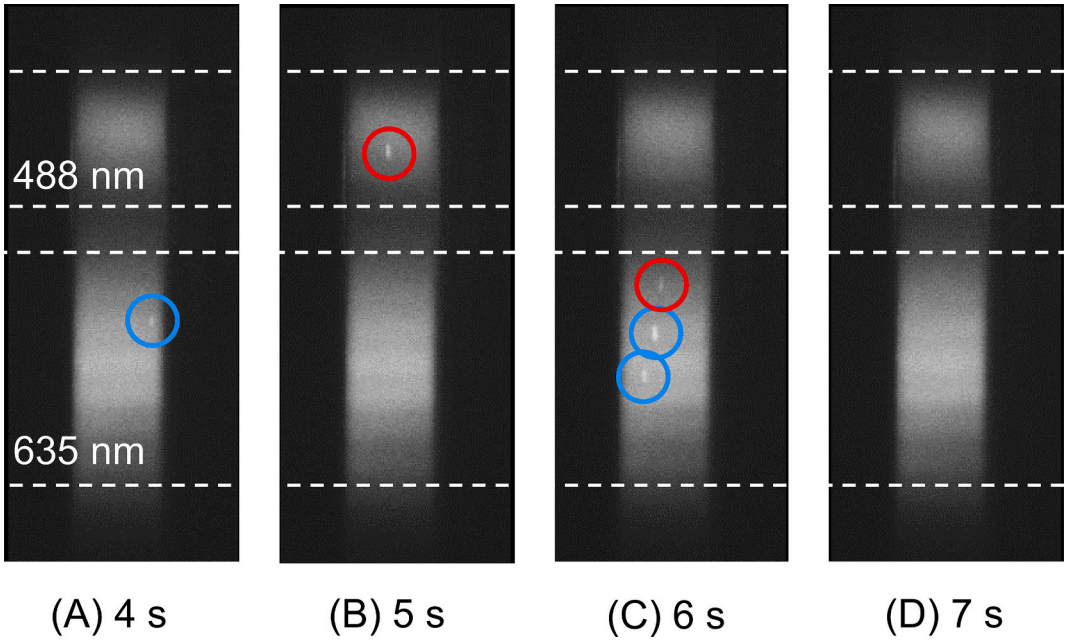

Fig. 6. Images for the detection of two different EVs. The EVs surrounded by blue lines emitted upon 635-nm excitation at 4 and 6 s. The EVs surrounded by red lines emitted upon 488-nm excitation at 5 s and 635-nm excitation at 6 s. The EVs that emitted only upon 635-nm excitation were designated as "other" EVs, whereas the EVs emitting upon both 488-and 635-nm excitation were designated as CD63-positive EVs. (For interpretation of the references to color in this figure legend, the reader is referred to the web version of this article.)

detected in exosomes [30]. Actually, many previous studies report that both HeLa and A549 cells release EVs containing CD63 [31–34]. Therefore, we selected CD63 as a marker protein of EVs released from HeLa and A549 cells. However, we must note that the detected EVs might not exactly be exosomes because CD63 alone cannot identify exosomes. Thus, they are defined as CD63-positive EVs, albeit not exosomal EVs.

Fig. 5 shows anti-CD63-PE bound to CD63 on the CD63-positive EVs that emit under excitation at 488 nm, whereas the lipid-staining dye ExoSparkler binds to all EVs and emits in the deep red region when excited at 635 nm. Consequently, CD63-positive EVs are detected at the focal positions of both the 488 and 635 nm lasers, while other EVs emit fluorescence only at the focal position of the 635 nm laser. This enables the discrimination of CD63-positive EVs from other EV populations.

The proposed system was applied to the direct detection of EVs released by HeLa cells into the culture medium. EVs were dual-labeled with anti-CD63-PE and a membrane-staining dye, and their fluorescence signals were analyzed using excitation at 488 and 635 nm. The detection process is depicted in Fig. 6 showing how EVs were detectable despite the high levels of background signals appearing at the regions where the lasers were focused because of the presence of free anti-CD63-PE and free lipid-staining dye in the sample solution. The signal-to-noise ratios at the 488 and 635-nm regions were estimated to be 4.3 and 3.2 in the presence of free dyes, respectively, based on the signal intensity and background fluctuations. These values indicate that EV-derived fluorescence signals are reliably distinguished from background noise under the present experimental conditions.

At 4 s, fluorescence was detected from an EV excited by the 635 nm laser. Since this EV showed no detectable fluorescence under 488 nm excitation at earlier time points, it was identified as a non-CD63-positive EV. By contrast, a CD63-positive EV was first detected at 5 s as it passed through the 488 nm laser beam and then reappeared at 6 s under 635 nm excitation. At the same 6 s mark, two additional EVs were observed; however, these were not visible under 488 nm excitation for either 4 or 5 s, which indicated an absence of anti-CD63-PE binding. Thus, these vesicles were also classified as non-CD63-positive EVs. A corresponding video is provided in Supplementary video S2.

A limitation of this study is the presence of nonspecific staining and unbound fluorescent probes. Although purification methods such as ultrafiltration or size-exclusion chromatography could remove free dyes, these processes could also result in the loss of nanosized vesicles and altered particle counts. Thus, to preserve the native particle population, no additional purification step was performed after staining. Therefore, the contribution of nonspecific signals cannot be completely excluded, although signal discrimination based on temporal characteristics was applied. Future work will focus on optimizing purification and labeling strategies to improve specificity.

The trajectories of EVs were tracked by analyzing each frame of the movie provided in the Supplementary video S2, as illustrated in Fig. 7. An EV first appeared at 5.4 s under 488 nm excitation. At 5.8 s, the EV emitted fluorescence within the boundary region of the two laser beams, where two additional EVs simultaneously appeared. Because these two EVs were not observed before 5.8 s, they are unlikely to be bound to anti-CD63-PE. At 6.2 s, all three EVs exhibited fluorescence under 635 nm excitation. Therefore, the EVs enclosed by red lines were identified as CD63-positive EVs, whereas those enclosed by blue lines were classified as other EVs. As shown in Fig. 7, fluorescence emission observed in the boundary region allowed the continuous tracking of EV trajectories.

The numbers of CD63-positive and non-CD63-positive EVs released from HeLa and A549 cells are summarized in Tables 2 and 3, respectively. Experiments were conducted on two separate days for each cell line. The overall counts and ratios of CD63-positive EVs and other EVs were consistent across both days. Although the numbers of both types of vesicles fluctuated between the two days, this variation could be attributed to differences in cell proliferation rates due to passaging [35], which could have affected both cell density and EV production.

The proportion of CD63-positive EVs in the total EV population was approximately 3% for HeLa cells and 9% for A549 cells. However, a significant difference was observed in the numbers of other types of EVs between the two cell lines. Although cell numbers were measured for each sample, the difference in cell count (16.7×10^4 for HeLa and 9.4×10^4 for A549) was not as pronounced as the variation in vesicle numbers (Average of other types of EVs shown in Tables 3 and 4: 550 for HeLa and 65 for A549). This discrepancy could be associated with cancer cell

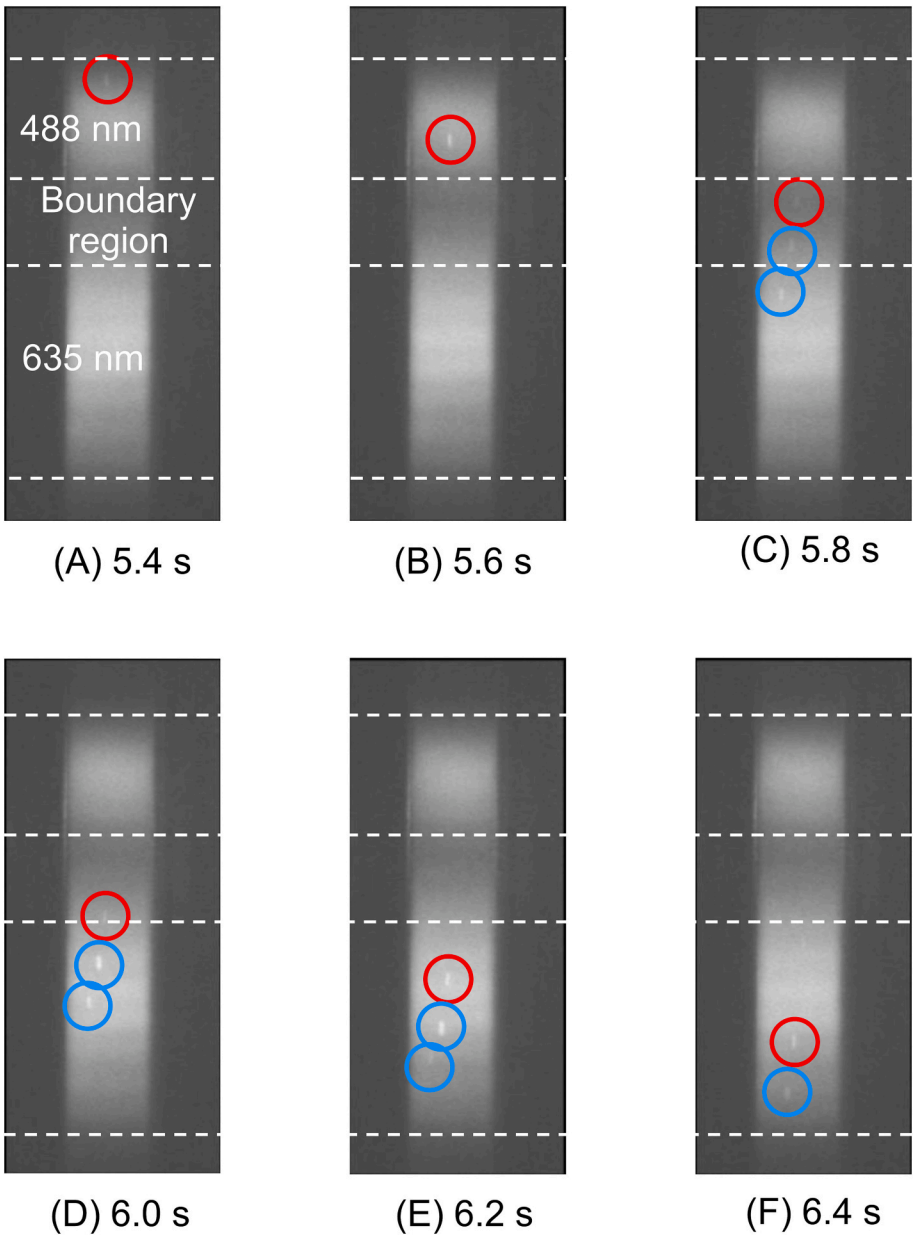

Fig. 7. Images for the trajectory of two different EVs. As the EVs passed sequentially through the 488-nm region, the boundary, and the 635-nm region, those surrounded by blue lines emitted only at the boundary and 635-nm region between 5.8 and 6.4 s. On the other hand, the EVs surrounded by red lines emitted throughout all regions from 5.4 to 6.4 s. (For interpretation of the references to color in this figure legend, the reader is referred to the web version of this article.)

Table 2
Number of CD63-positive EVs and other EVs released from HeLa cells on different days.

	Day 1	Day 2
CD63-positive EVs	20 ± 1	16 ± 1
Other EVs	530 ± 21	569 ± 10
Ratio of CD63-positive EVs/ %	3.6	2.6

Table 3
Number of CD63-positive EVs and other EVs released from A549 cells on different days.

	Day 1	Day 2
CD63-positive EVs	6 ± 1	7 ± 1
Other EVs	58 ± 4	72 ± 1
Ratio of CD63-positive EVs/ %	9	9

malignancy and cellular processes. Previous studies have shown that highly malignant cancer cells release EVs with a higher protein content compared with those derived from patients with less-malignant diseases or from healthy individuals [36]. Additionally, the release of EVs is influenced by biological processes such as cell activation and cell death, with the latter causing a substantial increase in EV concentration at the end of the bioprocess [37]. These findings suggest that different cell lines produce varying amounts of EVs. Although the proportion of CD63-positive EVs was relatively low, this could reflect the heterogeneous expression of CD63 among EV subpopulations, in addition to technical factors such as labeling efficiency and detection sensitivity. Further investigation of these underlying mechanisms remains a subject for future study, as it is beyond the scope of this work.

Table 4
Effect of doxorubicin on the secretion of EVs.

Cell		Concentration of doxorubicin			
		0 μM	0.5 μM	1.5 μM	3.0 μM
HeLa	CD63-positive EVs	19 ± 1	30 ± 1	47 ± 1	56 ± 1
	Other EVs	576 ± 10	834 ± 19	1093 ± 59	1114 ± 79
	Cell ($\times 10^4$)	14.2	4.0	2.0	1.0
	Ratio of CD63-positive EVs/ %	3.2	3.5	4.1	4.8
A549	CD63-positive EVs	8 ± 2	41 ± 1	340 ± 19	352 ± 18
	Other EVs	64 ± 14	238 ± 14	890 ± 34	932 ± 57
	Cell ($\times 10^4$)	10.9	2.6	1.7	1.5
	Ratio of CD63-positive EVs / %	11	15	28	27

Table 5
p-values at a confidential level of 95% for EVs.

	p-value			
	Type of EVs	0 and 0.5 μM	0.5 and 1.5 μM	1.5 and 3.0 μM
HeLa	CD63-positive EVs	0.0003	0.00003	0.000005
	Other EVs	0.00008	0.0003	0.7
A549	CD63-positive EVs	0.00002	0.00003	0.6
	Other EVs	0.0002	0.00002	0.3

3.3. Influence of an anticancer drug on the release of EVs

We also examined the effect of the anticancer drug doxorubicin on EV secretion. Doxorubicin was added to the culture medium in concentrations of 0.5, 1.5, and 3.0 μM. Table 4 presents the number of cells, CD63-positive EVs, other EVs, and the ratio of CD63-positive EVs to other EVs for both HeLa and A549 cells. As expected, doxorubicin treatment resulted in a dose-dependent reduction in cell numbers (Supplementary materials, Figs. S5 and S6). As the handheld cell counter used in this study cannot distinguish between live, dead, or apoptotic cells, the underlying mechanism of this decrease was not directly assessed. These results are consistent with trends reported in previous studies that assessed the viability of HeLa and A549 cells [38,39]. Li et al. reported that cell viability in both HeLa and A549 cells decreased with increasing doxorubicin concentration, as determined using a Cell Counting Kit-8 assay [39]. Their results also showed that cell viability fell below 50% at a doxorubicin concentration of 1.5 μM after 24 h. Although our measurements are based on cell number rather than direct viability assays, the overall trend is in agreement with these previous findings.

The *p*-values between the number of EVs at different concentrations of doxorubicin are shown in Table 5. The p-values are smaller than 0.05 in the concentrations between 0 and 0.5 μM and between 0.5 and 1.5 μM, implying that the number of EVs is significantly different. Conversely, between 1.5 and 3.0 μM, a significant difference was observed only for the CD63-positive EVs from HeLa cells. These results imply that doxorubicin induces an increase in the number of EVs at a lower concentration, while the number of EVs would be saturated at a high concentration.

Notably, not only did the total number of EVs increase, but the ratio of CD63-positive EVs also rose with increases in drug concentration. This observation aligns with previous reports that anticancer agents, including doxorubicin, stimulate EV release [40,41], which supports the validity of the results, as shown in Table 4.

HeLa cells released a greater total number of EVs compared with the total released by A549 cells. However, the proportion of CD63-positive EVs was consistently higher in A549 cells. The ratio of CD63-positive EVs to other EVs showed no significant change across doxorubicin concentrations (0.5–3.0 μM) within each cell line. However, the ratio was significantly higher in A549 cells than in HeLa cells (20 ± 9 vs. 3.9 ± 0.7, mean ± SD, $n = 4$, $p = 0.03$, *t*-test). The proposed simple and inexpensive system is potentially applicable to monitoring changes in both the numbers and types of EVs.

4. Conclusions

The present study demonstrated that a laser-induced fluorescence detection system comprised of two lasers could be used to effectively differentiate between two types of liposomes and EVs. The two lasers of this system emit at 488 and 635 nm to individually detect nanometer-sized vesicles labeled with dyes excitable at these respective wavelengths. Quantitative discrimination between Rhod-labeled and Atto-labeled liposomes was confirmed based on fluorescence signals, and this result is consistent with the expected mixing ratios. However, we should note that this study has several limitations. First, detailed physicochemical characterization of the liposomes, including size distribution, zeta potential, and fluorescent labeling efficiency, was not performed. Although fluorescent lipids were homogeneously mixed prior to liposome formation, the actual labeling efficiency at the single-liposome level was not directly evaluated. Therefore, potential variability in fluorescence intensity among liposomes cannot be completely excluded. Nevertheless, as the present analysis is based on relative comparisons under identical preparation conditions, such variability is unlikely to affect the main conclusions. Future studies incorporating detailed physicochemical characterizations will further strengthen these findings.

Furthermore, the detection system successfully distinguished CD63-positive EVs from other EVs by employing a labeled anti-CD63 antibody and a non-selective membrane staining dye. Quantitative analysis of the labeled EVs suggested that HeLa and A549 cells secreted 3 and 9% of the CD63-positive EVs, respectively, relative to the total EV population. Additionally, the detection system was applied to evaluate the effect of the anticancer drug doxorubicin on EV secretion. In clinical applications, distinguishing EVs derived from cancer cells from those released by normal cells is an important challenge. However, the current technique still has difficulty achieving this distinction because both types of EVs often contain similar membrane proteins. Therefore, it is essential to identify marker proteins and the corresponding antibodies that are specifically expressed in EVs released from cancer cells. This detection system uses a facile and inexpensive instrument to discriminate among various biological vesicles based on membrane proteins, which confers significant potential provided that corresponding antibodies labeled with distinct fluorescent dyes are available. Furthermore, the implementation of a multi-laser system is expected to enhance recognition capabilities, as the number of distinguishable membrane proteins will increase with the incorporation of three or more excitation wavelengths.

Supplementary data to this article can be found online at https://doi.org/10.1016/j.saa.2026.127928.

Supplementary video S1, Detection of Rhod-labeled and Atto-labeled liposomes.

Supplementary video S2, Detection of CD63-positive EVs and "other" types of EVs.

Supplementary materials, Fig. S1. Optimization of the amounts of membrane dye; Fig. S2. The excitation and emission spectra of anti-CD63-PE and the membrane-labeling dye; Fig. S3. Images of water and liposomes without fluorescent labeling; Fig. S4. Calibration curves of liposomes; Fig. S5. Images of HeLa cells after incubation with doxorubicin; Fig. S6. Images of A549 cells after incubation with doxorubicin.

Declaration of competing interest

The authors declare that they have no known competing financial interests or personal relationships that could have appeared to influence the work reported in this paper.

Acknowledgements

This work was supported by the Japan Society for Promotion of Science (JSPS) KAKENHI Grant Numbers JP25K01800.

Data availability

Data will be made available on request.

References

[1] J.A. Welsh, D.C. Gobert, L. O'Driscoll, et al., Minimal information for studies of extracellular vesicles 2023 (MISEV2023): from basic to advanced approaches, J. Extracell. Vesicles 13 (2024) e12404, https://doi.org/10.1002/jev2.12404.
[2] Y. Qin, L. Zhang, X. Wang, et al., Recent advances in extracellular vesicle-based drug delivery systems, Pharmaceutics 17 (2025) 1550, https://doi.org/10.3390/pharmaceutics17121550.
[3] R. Kalluri, V. Le Bleu, The biology, function, and biomedical applications of exosomes, Science 367 (2020) eaau6977, https://doi.org/10.1126/science.aau6977.
[4] Y. Xing, Z. Cheng, R. Wang, C. Lv, T.D. James, F. Yu, Analysis of extracellular vesicles as emerging theranostic nanoplatforms, Coord. Chem. Rev. 424 (2020) 213506, https://doi.org/10.1016/j.ccr.2020.213506.
[5] X. Chen, J. Tang, Y. Zhao, R. Wang, S. Sang, F. Yu, Y. Xing, Sensitive phenotyping of serum extracellular vesicles on a SERS-microfluidic platform for early-stage clinical diagnosis of ovarian carcinoma, Biosens. Bioelectron. 267 (2025) 116724, https://doi.org/10.1016/j.bios.2024.116724.
[6] R.J. Simpson, S.S. Jensen, J.W. Lim, Proteomic profiling of exosomes: current perspectives, Proteomics 8 (2008) 4083–4099, https://doi.org/10.1002/pmic.200800109.
[7] M. Lan, Y. Zhang, Y. Chen, Solving the contamination conundrum derived from coisolation of extracellular vesicles and lipoproteins: approaches for isolation and characterization, Small Methods 9 (2025) e01606, https://doi.org/10.1002/smtd.202501606.
[8] F. Momen-Heravia, L. Balaja, S. Alian, P.-Y. Mantel, A.E. Halleck, A. J. Trachtenberg, C.E. Soria, S. Oquin, C.M. Bonebreak, E. Saracoglu, J. Skog, W. P. Kuo, Current methods for the isolation of extracellular vesicles, Biol. Chem. 394 (2013) 1253–1262, https://doi.org/10.1515/hsz-2013-0141.
[9] P. Li, M. Kaslan, S.H. Lee, J. Yao, Z. Gao, Progress in exosome isolation techniques, Theranostics 7 (2017) 789–804, https://doi.org/10.7150/thno.18133.
[10] F. Yang, X. Liao, Y. Tian, G. Li, Exosome separation using microfluidic systems: size-based, immunoaffinity-based and dynamic methodologies, Biotechnol. J. 12 (2017) 1600699, https://doi.org/10.1002/biot.201600699.
[11] S. Lin, Z. Yu, D. Chen, Z. Wang, J. Miao, Q. Li, D. Zhang, J. Song, D. Cui, Progress in microfluidics-based exosome separation and detection technologies for diagnostic applications, Small 16 (2020) e1903916, https://doi.org/10.1002/smll.201903916.
[12] S. Lima Moura, M. Martì, M.I. Pividori, Matrix effect in the isolation of breast cancer-derived nanovesicles by immunomagnetic separation and electrochemical immunosensing-a comparative study, Sensors (Basel) 20 (2020) 965, https://doi.org/10.3390/s20040965.
[13] R. Xu, A. Fitts, X. Li, J. Fernandes, R. Pochampally, J. Mao, Y.M. Liu, Quantification of small extracellular vesicles by size exclusion chromatography with fluorescence detection, Anal. Chem. 88 (2016) 10390–10394, https://doi.org/10.1021/acs.analchem.6b03348.
[14] M. Kuboi, N. Takeyasu, T. Kaneta, Enhanced optical collection of micro- and nano-vesicles in the presence of gold nanoparticles, ACS Omega 3 (2018) 2527–2531, https://doi.org/10.1021/acsomega.8b00033.
[15] Y. Tani, T. Kaneta, Enhancement of optical force acting on vesicles via the binding of gold nanoparticles, Royal Soc. Open Sci. 6 (2019) 190293, https://doi.org/10.1098/rsos.190293.
[16] Y. Tani, K. Ochiai, T. Kaneta, Optical collection of extracellular vesicles in a culture medium enhanced by interactions with gold nanoparticles, Anal. Sci. 39 (2023) 643–651, https://doi.org/10.1007/s44211-022-00207-2.
[17] J. Chen, P. Li, T. Zhang, Z. Xu, X. Huang, R. Wang, L. Du, Review on strategies and technologies for exosome isolation and purification, Front. Bioeng. Biotechnol. 9 (2022) 811971, https://doi.org/10.3389/fbioe.2021.811971.
[18] J. Lai, Z. Chau, S. Chen, J. Hill, K. Korpany, N. Liang, L. Lin, Y. Lin, J. Liu, Y. Liu, R. Lunde, W. Shen, Exosome processing and characterization approaches for research and technology development, Adv. Sci. 9 (2022) 2103222, https://doi.org/10.1002/advs.202103222.
[19] H. Shao, H. Im, C.M. Castro, X. Breakefield, R. Weissleder, H. Lee, New technologies for analysis of extracellular vesicles, Chem. Rev. 118 (2018) 1917–1950, https://doi.org/10.1021/acs.chemrev.7b00534.
[20] E. Serrano-Pertierra, M. Oliveira-Rodríguez, M. Matos, G. Gutiérrez, A. Moyano, M. Salvador, M. Rivas, M.C. Blanco-López, Extracellular vesicles: current analytical techniques for detection and quantification, Biomolecules 28 (2020) 824, https://doi.org/10.3390/biom10060824.
[21] Z. Zhao, H. Wijerathne, A.K. Godwin, S.A. Soper, Isolation and analysis methods of extracellular vesicles (EVs), Extracell. Vesicles Circ. Nucl. Acids 2 (2021) 80–103, https://doi.org/10.20517/evcna.2021.07.
[22] A. Hendrix, L. Lippens, C. Pinheiro, C. Théry, L. Martin-Jaular, J. Lötvall, C. Lässer, A.F. Hill, K.W. Witwer, Extracellular vesicle analysis, Nat. Rev. Methods Primers 3 (2023) 56, https://doi.org/10.1038/s43586-023-00240-z.
[23] L. Alexandre, J. Sun, M. Taverna, W. Zhong, Advances in extracellular vesicle analysis, Anal. Bioanal. Chem. 415 (2023) 1235–1238, https://doi.org/10.1007/s00216-023-04536-7.
[24] Z. Wang, X. Zhou, Q. Kong, H. He, J. Sun, W. Qiu, L. Zhang, M. Yang, Extracellular vesicle preparation and analysis: a state-of-the-art review, Adv. Sci. 11 (2024) 2401069, https://doi.org/10.1002/advs.202401069.
[25] R.A. Dragovic, C. Gardiner, A.S. Brooks, D.S. Tannetta, D.J.P. Ferguson, P. Hole, B. Carr, C.W.G. Redman, A.L. Harris, P.J. Dobson, P. Harrison, I.L. Sargentm, Sizing and phenotyping of cellular vesicles using nanoparticle tracking analysis, Nanomed. Nanotechnol. Biol. Med. 7 (2011) 780–788, https://doi.org/10.1016/j.nano.2011.04.003.
[26] H. Joung, G.J. Jang, J.Y. Jeong, G. Lim, S.Y. Han, Evaluating the in situ effects of whole protein coronas on the biosensing of antibody-immobilized nanoparticles using two-color fluorescence nanoparticle tracking analysis, Nanomaterials (Basel) 30 (2025) 220, https://doi.org/10.3390/nano15030220.
[27] J. Maia, S. Batista, N. Couto, A.C. Gregório, C. Bodo, J. Elzanowska, M.C. Strano Moraes, B. Costa-Silva, Employing flow cytometry to extracellular vesicles sample microvolume analysis and quality control, Front. Cell Dev. Biol. 8 (2020) 593750, https://doi.org/10.3389/fcell.2020.593750.
[28] T. Fujii, T. Kaneta, Direct counting of exosomes in a cell culture medium using neither isolation nor preconcentration, Anal. Chim. Acta 1119 (2020) 35–40, https://doi.org/10.1016/j.aca.2020.04.052.
[29] T. Anazawa, H. Matsunaga, E.S. Yeung, Electrophoretic quantitation of nucleic acids without amplification by single-molecule imaging, Anal. Chem. 74 (2002) 5033–5038, https://doi.org/10.1021/ac025801u.
[30] Z. Song, J. Mao, R.A. Barrero, P. Wang, F. Zhang, T. Wang, Development of a CD63 aptamer for efficient cancer immunochemistry and immunoaffinity-based exosome isolation, Molecules 25 (2020) 5585, https://doi.org/10.3390/molecules25235585.
[31] M. Mathieu, N. Névo, M. Jouve, J.I. Valenzuela, M. Maurin, F.J. Verweij, R. Palmulli, D. Lankar, F. Dingli, D. Loew, E. Rubinstein, G. Boncompain, F. Perez, C. Théry, Specificities of exosome versus small ectosome secretion revealed by live intracellular tracking of CD63 and CD9, Nat. Commun. 12 (2021) 4389, https://doi.org/10.1038/s41467-021-24384-2.
[32] M. Ruzycka-Ayoush, A.M. Nowicka, A. Kowalczyk, A. Gluchowska, A. Targonska, G. Mosieniak, K. Sobcza, M. Donten, I.P. Grudzinski, Exosomes derived from lung cancer cells: isolation, characterization, and stability studies, Eur. J. Pharm. Sci. 181 (2023) 106369, https://doi.org/10.1016/j.ejps.2022.106369.
[33] H. Balbinotti, N.A. Cadore, C.S. Dutra, E.D. Da Silva, H.B. Ferreira, A. Zaha, K. M. Monteiro, Protein profiling of extracellular vesicles associated with cisplatin resistance in lung cancer, Anticancer Res 40 (2020) 5509–5516, https://doi.org/10.21873/anticanres.14563.
[34] A. Giannopoulos-Dimitriou, A. Saiti, A. Malousi, A.K. Anagnostopoulos, G. Vatsellas, P.M. Al-Maghrabi, A. Müllertz, D.G. Fatouros, I.S. Vizirianakis, Molecular profiling of a549 cell-derived exosomes: proteomic, miRNA, and interactome analysis for identifying potential key regulators in lung cancer, Cancers (Basel) 16 (2024) 4123, https://doi.org/10.3390/cancers16244123.
[35] W. Jin, C.J. Penington, S.W. McCue, M.J. Simpson, A computational modelling framework to quantify the effects of passaging cell lines, PloS One 12 (2017) e0181941, https://doi.org/10.1371/journal.pone.0181941.
[36] A. Ortiz, Extracellular vesicles in cancer progression, Semin. Cancer Biol. 76 (2021) 139–142, https://doi.org/10.1016/j.semcancer.2021.05.032.
[37] A.B. Zavec, V. Kralj-Iglič, M. Brinc, T.F. Trček, D. Kuzman, A. Schweiger, G. Anderluh, Extracellular vesicles concentration is a promising and important parameter for industrial bioprocess monitoring, Biotechnol. J. 11 (2016) 603–609, https://doi.org/10.1002/biot.201500049.
[38] X. Tai, X.B. Cai, Z. Zhang, R. Wei, In vitro and in vivo inhibition of tumor cell viability by combined dihydroartemisinin and doxorubicin treatment, and the underlying mechanism, Oncol. Lett. 12 (2016) 3701–3706, https://doi.org/10.3892/ol.2016.5187.
[39] S. Li, X. Chen, H. Chen, J. Peng, X. Yang, Small peptide-doxorubicin co-assembly for synergistic cancer therapy, Molecules 25 (2020) 484, https://doi.org/10.3390/molecules25030484.
[40] L.H. Lv, Y.L. Wan, Y. Lin, W. Zhang, M. Yang, G.L. Li, H.M. Lin, C.Z. Shang, Y. J. Chen, J. Min, Anticancer drugs cause release of exosomes with heat shock proteins from human hepatocellular carcinoma cells that elicit effective natural killer cell antitumor responses in vitro, J. Biol. Chem. 287 (2012) 15874–15885, https://doi.org/10.1074/jbc.M112.340588.
[41] S.E. Emam, H. Ando, A.S. Abu Lila, S. Kobayashi, T. Shimizu, K. Okuhira, Y. Ishima, T. Ishida, Doxorubicin expands in vivo secretion of circulating exosome in mice, Biol. Pharm. Bull. (2018) 1078–1083, https://doi.org/10.1248/bpb.b18-00202.